GLOBULAR CLUSTER STAR CLASSIFICATION: APPLICATION TO M13

R. Caimmi

Dipartimento di Fisica e Astronomia, Università di Padova
Vicolo Osservatorio 3/2, I-35122 Padova, Italy

E–mail: *roberto.caimmi@unipd.it*

SUMMARY: Starting from recent determination of Fe, O, Na abundances on a restricted sample $(N = 67)$ of halo and thick disk stars, a natural and well motivated selection criterion is defined for the classification globular cluster stars. An application is performed to M13 using a sample $(N = 113)$ for which Fe, O, Na abundances have been recently inferred from observations. A comparison is made between the current and earlier M13 star classifications. Both O and Na empirical differential abundance distributions are determined for each class and for the whole sample (with the addition of Fe in the last case) and compared with their theoretical counterparts due to cosmic scatter obeying a Gaussian distribution whose parameters are inferred from related subsamples. The occurrence of an agreement between the empirical and theoretical distributions is interpreted as absence of significant chemical evolution and vice versa. The procedure is repeated with regard to four additional classes depending on whether oxygen and sodium abundance is above (stage CE) or below (stage AF) a selected threshold. Both O and Na empirical differential abundance distributions, related to the whole sample, exhibit a linear fit for the AF and CE stage. Within the errors, the oxygen slope for the CE stage is equal and of opposite sign with respect to the sodium slope for AF stage, while the contrary holds when dealing with the oxygen slope for the AF stage with respect to the sodium slope for the CE stage. In the light of simple models of chemical evolution applied to M13, oxygen depletion appears to be mainly turned into sodium enrichment for [O/H]≥ -1.35 and [Na/H]≤ -1.45, while one or more largely preferred channels occur for [O/H]< -1.35 and [Na/H]> -1.45. In addition, the primordial to the current M13 mass ratio can be inferred from the true sodium yield in units of the sodium solar abundance. Though the above results are mainly qualitative due to large $(\mp 1.5$ dex$)$ uncertainties in abundance determination, still the exhibited trend is expected to be real. The proposed classification of globular cluster stars may be extended in a twofold manner, namely to: (i) elements other than Na and Fe and (ii) globular clusters other than M13.

Key words. Galaxy: evolution - Galaxy: formation - Galaxy: halo - globular clusters: general - globular clusters: individual (M13).

1. INTRODUCTION

Globular clusters (GCs) are fundamental building blocks of galaxies and most of them are among the oldest stellar systems. Abundance analysis of GC stars provides valuable clues for understanding the evolution of both the cluster itself and the hosting galaxy.

In the past, GCs were conceived as a result of an initial burst of highly efficient star formation, where the remaining gas was blown up by type II supernovae (SNII) explosions together with SNII ejecta. Gas returned later from planetary nebulae was blown up by type Ia supernovae (SNIa) explosions together with SNIa ejecta. Accordingly, GC stars were expected to be coeval and with element abundance affected only by cosmic scatter.

Abundance surveys with increasingly precise instrumentation revealed consistent star-to-star abundance variation of light elements (from C to Al). At least in several cases, significant variations in He abundance were inferred. For further details and complete references, an interested reader is addressed to recent comprehensive GC abundance surveys (e.g. Carretta et al. 2009a, 2009b), reviews (e.g. Piotto 2009, Gratton et al. 2012) and investigations (e.g. Johnson and Pilachowski 2012, hereafter quoted as JP12; Conroy 2012, hereafter quoted as C12).

More specifically, interpretation of recent data disclosed the following. (i) GC normal (i.e. similar photospheric composition with respect to field halo stars) and anomalous (i.e. different photospheric composition with respect to field halo stars) stars affect the total mass to a comparable extent. (ii) Light element abundance undergoes a continuous variation passing from GC normal to most anomalous stars. (iii) GC anomalous stars exhibit enhanced N, Na, Al; depleted O, Mg; more or less unchanged Si, Ca, Fe; enhanced He; anticorrelations such as O-Na, Mg-Al; multiple evolutionary sequences in the colour-magnitude diagram.

An explanation of the above mentioned findings, within the framework of a single model, is not an easy matter. For instance, GC normal and anomalous stars in comparable proportion would imply more massive GCs at birth and/or substantially different initial stellar mass function if anomalous abundances are due to the asymptotic giant branch (AGB) stars ($3 \overset{<}{\sim} m/m_\odot \overset{<}{\sim} 8$); a continuous variation of light elements passing from GC normal to most anomalous stars would imply (at least) two star generations separated by a time interval longer than about 0.1 Gyr and, in addition, inhomogeneous mixing between the recycled material from AGB stars and inflowing primordial gas, or could be a mere effect of mesaurement errors; O-Na and Mg-Al anticorrelations, together with enhanced He, would imply high-temperature proton-capture burning within AGB stars and/or rapidly rotating massive main-sequence stars and/or massive binary stars; for further details and complete references an interested reader is addressed to recent investigations (e.g. JP12; C12) and proceedings (e.g. Cassisi et al. 2013, Renzini 2013, Ventura et al. 2013).

GC anomalous stars are usually subclassified as extreme and intermediate, depending on whether light elements are substantially or moderately enhanced/depleted with respect to field halo stars of similar Fe abundance (e.g. JP12). On the other hand, no general consensus still exists about a definition of GC normal (or primordial), intermediate and extreme stars, due to absence of a related physical criterion for distinguishing ones from the others. A rigorous GC star classification would be useful for tracing the past history of the Galaxy and, in fact, it can be made using recent abundance determinations available for a sample of halo and low-metallicity ([Fe/H] < −0.6) thick disk stars (Nissen and Schuster 2010, hereafter quoted as NS10; Ramirez et al. 2012, hereafter quoted as Ra12).

The present note is aimed to this respect, with special effort devoted to O, Na, Fe, whose abundances are known for about one hundred M13 stars (JP12). Following a current attempt (Caimmi 2013), a rigorous GC star classification is provided in Section 2. An application to M13, including both the star classification and differential element abundance distribution, is presented in Section 3. The implications for halo formation and evolution, in the light of a simple model of chemical evolution, are discussed in Section 4. The conclusion is outlined in Section 5.

2. A RIGOROUS GC STAR CLASSIFICATION

The fractional logarithmic number abundance or, in short, number abundance, can be inferred from recently studied samples of solar neighbourhood FGK-type dwarf stars (NS10; Ra12), as [Q/H]=[Q/Fe]−[Fe/H], for Q = O, Na, Mg, Si, Ca, Ti, Cr, Fe, Ni. More specifically, sample (HK) stars can be subsampled as low-α halo (LH), high-α halo (HH), thick disk (KD), GC outliers (OL). The related population is $N = 67$ (HK), 24 (LH), 25 (HH), 16 (KD), 2 (OL). Oxygen can be taken as reference element in that it is the most abundant metal and, in addition, synthesised mainly within SNII progenitors.

With regard to the (O [O/H] [Q/H]) plane, stars belonging to different environments are displayed along a "main sequence", [Q,O] = $[a_Q, b_Q, \Delta b_Q]$, bounded by two parallel straight lines:

$$[Q/H] = a_Q[O/H] + b_Q \mp \frac{1}{2}\Delta b_Q \ ; \qquad (1)$$

with the possible exception of OL stars. For further details refer to a current attempt (Caimmi 2013).

Aiming to an application to M13, where O, Na, Fe number abundances have recently been determined for about one hundred stars (JP12), the current investigation will be restricted to Q = Na, Fe, keeping in mind that it can be extended to any element whose number abundances are available for a large star sample. The main sequences chosen for iron and sodium, [Fe,O] = [1.00, −0.45, 0.50] and [Na,O] = [1.25, −0.40, 0.60], are shown in Figs. 1 and 2, respectively, top left panels, together with data from LH (squares), HH (crosses), KD (saltires), OL ("at" symbols) subsamples, taken from a current attempt (Caimmi 2013). The selected slopes are a compromise between related regression lines (Caimmi 2013).
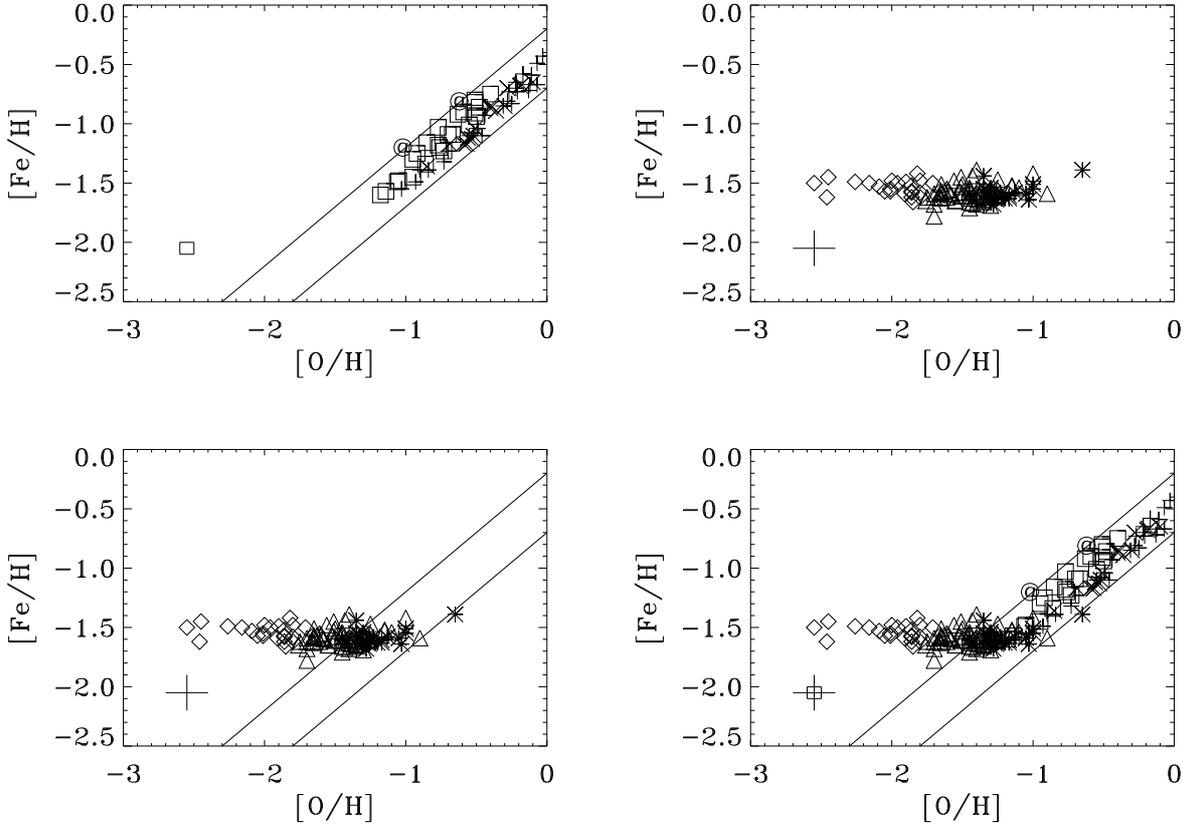
Fig. 1. *The selected main sequence, $[Fe/H] = [O/H] - 0.45 \mp 0.25$, together with the $[Fe/H]$-$[O/H]$ relation for LH (squares), HH (crosses), KD (saltires), OL ("at" symbols) populations, inferred (Caimmi 2013) from recent investigations (NS10; Ra12), top left panel; the $[Fe/H]$-$[O/H]$ relation for primordial (asterisks), intermediate (triangles), extreme (diamonds) M13 stars, inferred from recent subsampled data (JP12), top right panel; as in top right panel with the main sequence, $[Fe/H] = [O/H] - 0.45 \mp 0.25$, superimposed, bottom left panel; as in bottom left panel with LH, HH, KD, OL data superimposed, bottom right panel. Typical errors are represented by a cross (M13) and a square (LH, HH, KD, OL) when appropriate, on the bottom left of each panel. For further details refer to the text.*

GC stars are currently subsampled into three populations depending on whether the O-Na anticorrelation is absent, weak, strong, defined as primordial (P), intermediate (I), extreme (E), respectively (e.g. JP12). In general, GC stars are classified as normal if the element abundance is similar to their field halo counterparts with equal iron abundance, and anomalous otherwise (e.g. C12). In both cases, no general consensus still exists on the selection criterion.

With respect to the selected element, Q, let GC P stars be defined as those lying within the main sequence defined by field halo stars on the $(\mathrm{O}\,[O/H]\,[Q/H])$ plane, I stars as those lying within a parallel sequence towards still lower $[O/H]$, E stars as those lying within further parallel sequences towards lower $[O/H]$. The above mentioned selection criterion appears to be natural and well motivated,

in that it relates to the main sequence defined by field halo stars, as shown in Figs. 1 and 2, top left panels, for Q = Fe, Na, respectively. More specifically, the $(\mathrm{O}\,[O/H]\,[Q/H])$ plane could be divided into an infinite number of parallel sequences as:

$$[Q/H] = a_Q[O/H] + b_Q + \frac{2i \mp 1}{2}\Delta b_Q$$
$$i = 0, \mp 1, \mp 2, ... \qquad (2)$$

where $i = 0$ labels the main sequence populated by field halo stars, $i < 0$ and $i > 0$ label parallel sequences towards longer and lower $[O/H]$, respectively, for fixed $[Q/H]$. In this view, a generic GC star can be classified as belonging to a sequence labelled by an integer i with regard to a selected element Q.
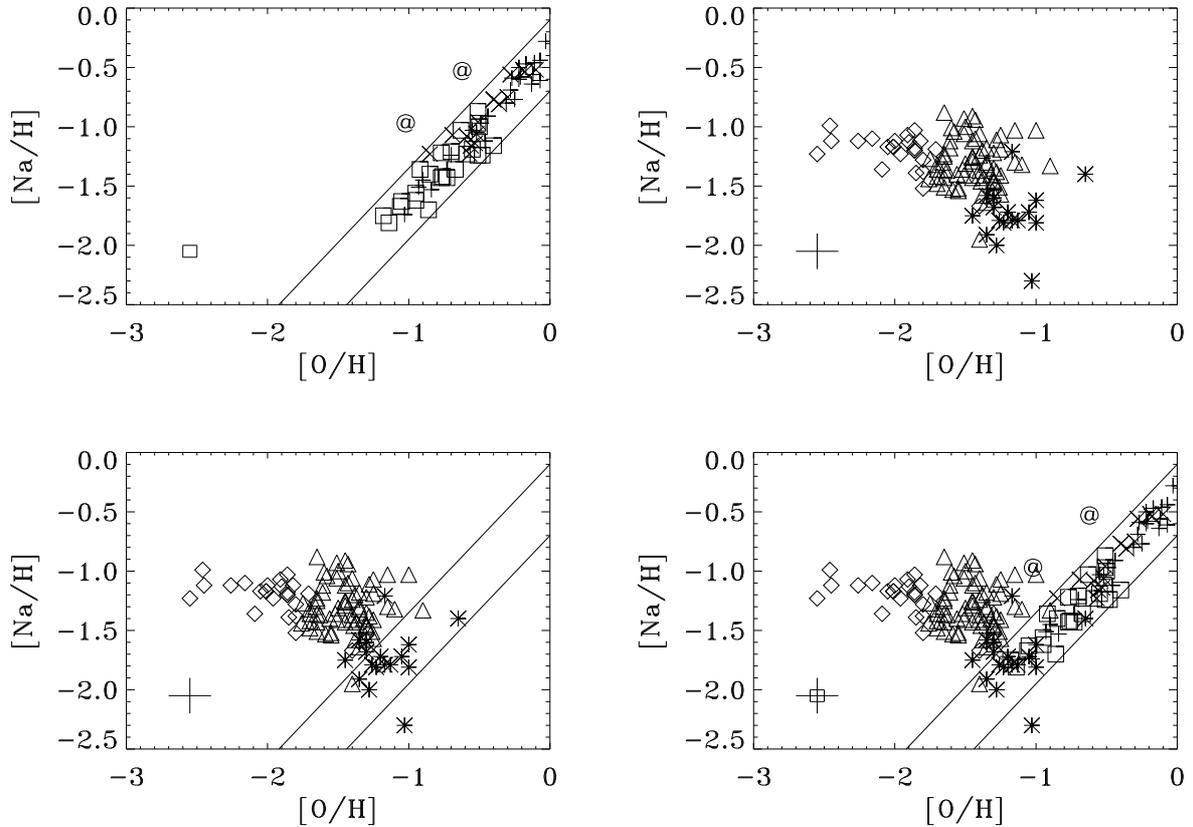
Fig. 2. *The selected main sequence, $[Na/H] = [O/H] - 0.4 \mp 0.3$, together with the $[Na/H]$-$[O/H]$ relation for LH (squares), HH (crosses), KD (saltires), OL ("at" symbols) populations, inferred (Caimmi 2013) from recent investigations (NS10; Ra12), top left panel; the $[Na/H]$-$[O/H]$ relation for primordial (asterisks), intermediate (triangles), extreme (diamonds) M13 stars, inferred from recent subsampled data (JP12), top right panel; as in top right panel with the main sequence, $[Na/H] = [O/H] - 0.4 \mp 0.3$, superimposed, bottom left panel; as in bottom left panel with LH, HH, KD, OL data superimposed, bottom right panel. Typical errors are represented by a cross (M13) and a square (LH, HH, KD, OL) when appropriate, on the bottom left of each panel. For further details refer to the text.*

3. APPLICATION TO M13

3.1. Star classification

Oxygen, sodium and iron abundances have recently been determined for a sample ($N = 113$) of red giant branch and AGB stars in M13 (JP12). Sample stars are divided therein into three classes according to the following prescriptions: $[Na/Fe] < 0.00$ - P; $[O/Fe] < 0.15$ - E; $[Na/Fe] \geq 0.00$ and/or $[O/Fe] \geq 0.15$ - I. For further details and exhaustive presentation, an interested reader is addressed to the parent paper (JP12). The following subsamples can be extracted from the parent sample: P ($N = 17$), I ($N = 70$), E ($N = 24$) where both $[O/Fe]$ and $[Na/Fe]$ are known with the exception of a (different) single star for both O and Na.

The related $[Q/H]$-$[O/H]$ relations, $Q = Fe$, Na, are plotted in Figs. 1, 2, respectively, top right panels, where P, I, E stars are represented by asterisks, triangles, diamonds, respectively. The main sequences, $[Fe,O] = [1.00, -0.45, 0.50]$, $[Na,O] = [1.25, -0.40, 0.60]$, are superimposed in bottom left panels of Figs. 1, 2, respectively. In addition, LH, HH, KD, OL stars (already shown in top left panels) are superimposed in bottom right panels of Figs. 1, 2, respectively.

An inspection of Fig. 1 reveals that, within the errors, P stars and a fraction of I stars lie inside the main sequence, $[Fe/H] = [O/H] - 0.45 \mp 0.25$ while the remining I stars together with E stars are located along a "horizontal branch", $[Fe/H] = -1.6 \mp 0.2$, which also comprises the above mentioned stars belonging to the main sequence, as shown in Fig. 3.
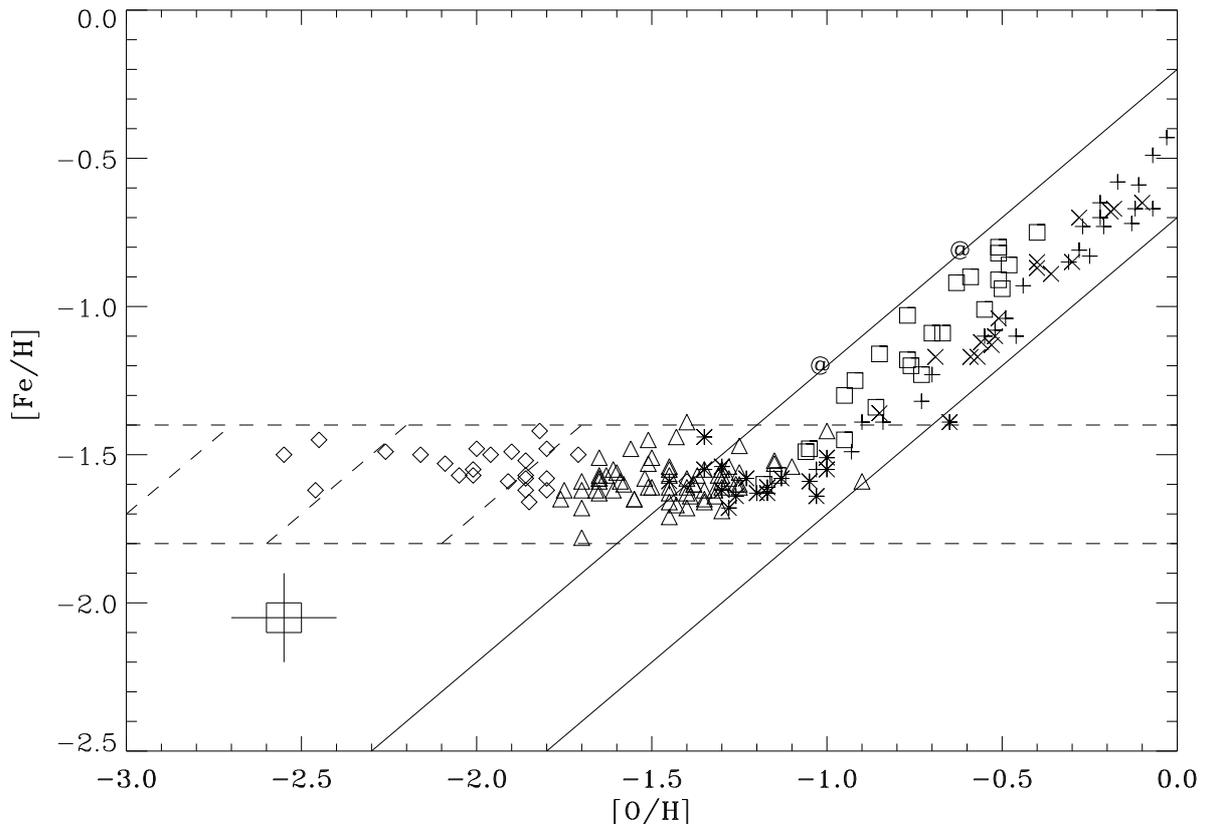
Fig. 3. *Zoom of Fig. 1, bottom right panel, where the parallel sequences, $[Fe/H] = [O/H]-0.45+(2i\mp1)0.25$, (class A_i), $i = 1, 2, 3$, and the horizontal branch, $[Fe/H] = -1.6\mp0.2$, are also plotted (dashed). M13 sample stars directly shift from the main sequence, $[Fe/H] = [O/H] - 0.45 \mp 0.25$, (class A_0), to the horizontal branch. For further details refer to the text.*

Accordingly, the following star classification can be made with respect to Fe: normal stars (class A_0) as those lying within the main sequence, $[Fe,O] = [1.00, -0.45, 0.50]$; anomalous stars (class A_i) as those lying within the parallel sequence, $[Fe/O] = [1.00, -0.45 + 0.50i, 0.50]$.

Let $([O/H],[Fe/H])$ be coordinates of a generic sample star on the $(O[O/H]$ $[Fe/H])$ plane. The straight line of unit slope passing through that point has the intercept $b_{Fe} = [Fe/H] - [O/H]$ and the related sequence is defined by the inequality:

$$-0.7 + 0.5i \leq b_{Fe} < -0.2 + 0.5i \qquad (3)$$

where $i = -1, 1, 2, 3$, in the case under discussion. It is worth noticing that M13 sample stars directly shift from the main sequence $[Fe/H] = [O/H] -0.45\mp0.25$ to the horizontal branch $[Fe/H] = -1.6\mp0.2$ as shown in Fig. 3.

An inspection of Fig. 2 discloses that, within the errors, a large fraction of P stars and a few I stars lie inside the main sequence $[Na/H] = 1.25 [O/H] -0.4 \mp 0.3$, the remining P, I, and almost all E stars

lie inside an inclined band which defines the O-Na anticorrelation, $[Na/H] = -0.8 [O/H]-2.5 \mp 0.7$, and ends on a horizontal branch $[Na/H] = -1.2 \mp 0.3$ as shown in Fig. 4.

Accordingly, the following star classification can be made with respect to Na: normal stars (class A_0) as those lying within the main sequence $[Na,O] = [1.25, -0.40, 0.60]$; anomalous stars (class A_i) lying within the parallel sequence $[Na/O] = [1.25, -0.40 + 0.60i, 0.60]$.

Let $([O/H],[Na/H])$ be coordinates of a generic sample star on the $(O[O/H]$ $[Na/H])$ plane. The straight line of slope $a_{Na} = 1.25$, passing through that point, has the intercept $b_{Na} = [Na/H] -1.25 [O/H]$, and the related sequence is defined by the inequality:

$$-0.7 + 0.6i \leq b_{Na} < -0.1 + 0.6i \qquad (4)$$

where $i = -1, 1, 2, 3, 4$, in the case under discussion. It is worth noticing that M13 sample stars shift from the main sequence $[Na/H] = 1.25 [O/H] -0.40\mp0.30$ to the horizontal branch $[Na/H] = -1.2 \mp 0.3$ via
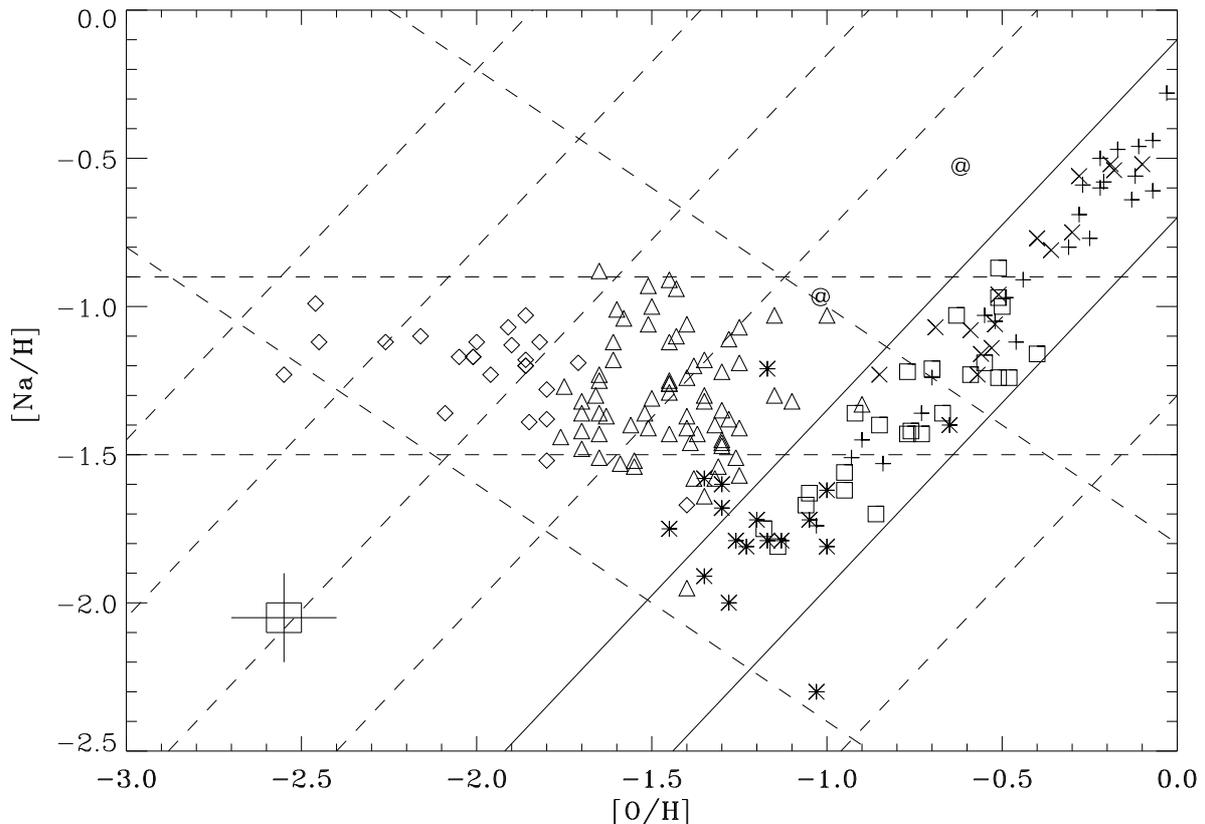
Fig. 4. *Zoom of Fig. 2, bottom right panel where the parallel sequences $[Na/H] = 1.25\,[O/H] - 0.40 + (2i \mp 1)0.30$ (class A_i) $i = -1, 1, 2, 3, 4$, the horizontal branch $[Na/H] = -1.2 \mp 0.3$, and the O-Na anticorrelation $[Na/H] = -0.8\,[O/H] - 2.5 \mp 0.7$ are also plotted (dashed). M13 sample stars shift from the main sequence $[Na/H] = 1.25[O/H] - 0.40 \mp 0.30$ (class A_0) to the horizontal branch via the parallel sequence $[Na/H] = 1.25[O/H] + 0.20 \mp 0.30$. For further details refer to the text.*

the parallel sequence $[Na/H] = 1.25\,[O/H] + 0.20 \mp 0.30$ as shown in Fig. 4. The O-Na anticorrelation, $[Na/H] = -0.8\,[O/H] - 2.5 \mp 0.7$, is also plotted therein.

An inspection of Figs. 3 and 4 suggests the following classification for M13 stars, which can be generalized to any GC where abundances have been determined for sufficiently large star samples. Let class N (normal stars), class T (transition stars), class H (horizontal branch stars), be defined in terms of subclasses as:

$$N = \sum_{i=-1}^{0} \sum_{j=-1}^{0} (A_i, A_j) \tag{5a}$$

$$T = \sum_{i=1}^{3} (A_i, A_0) + \sum_{j=1}^{4} (A_0, A_j) \tag{5b}$$

$$H = \sum_{i=1}^{3} \sum_{j=1}^{4} (A_i, A_j) \tag{5c}$$

where (A_i, A_j) relate to Fe and Na classification, respectively, of a selected sample star and the sum or the double sum extends over the whole set of possibilities for an assigned class. Accordingly, a selected sample star is defined by the coordinates, (A_i, A_j), $-1 \le i \le 3$, $-1 \le j \le 4$, i and j integers, where the first and the second place within parentheses relate to Fe and Na, respectively. The whole set of JP12 sample star data used in the current study is reported in Appendix A1.

The partition of star classes (A_i, A_j) into populations P, I, E, as defined in the parent paper (JP12), is shown in Table 1. The partition of star classes N, T, H, as defined by Eqs. (5), into populations P, I, E, is shown in Table 2.

Table 1. Partition of different M13 star populations according to the parent paper (JP12), P (primitive), I (intermediate), E (extreme), into classes with different degree of anomaly, A_i, $i = 0, \mp 1, \mp 2, ...$, with regard to Q = Fe, Na, as defined in the text. Class A_{-1} is listed as $-A_1$ for the sake of aesthetics.

pop:		P	I	E	all
Fe	Na				
$-A_1$	A_0	1	0	0	1
A_0	$-A_1$	1	0	0	1
A_0	A_0	9	2	0	11
A_0	A_1	3	25	0	28
A_0	A_2	0	5	0	5
A_1	A_0	1	0	0	1
A_1	A_1	2	7	1	10
A_1	A_2	0	30	4	34
A_1	A_3	0	1	3	4
A_2	A_2	0	0	1	1
A_2	A_3	0	0	11	11
A_2	A_4	0	0	1	1
A_3	A_4	0	0	3	3
all		17	70	24	111

Table 2. Partition of different M13 star populations according to the parent paper (JP12), P (primitive), I (intermediate), E (extreme), into classes N (normal), T (transition), H (horizontal branch), as defined in the text.

pop: class	P	I	E	all
N	11	2	0	13
T	4	30	0	34
H	2	38	24	64
all	17	70	24	111

It can be seen that class N hosts about two thirds of P stars together with a few I stars while class T hosts about one quarter of P stars and slightly less than one half of I stars. On the other hand, class H hosts a few P stars, slightly more than one half of I stars and all the E stars.

In conclusion, a classification of M13 sample stars as N, T, H, instead of P, I, E, seems more complete in that it includes both O, Fe, Na, and rigorous in that it is defined in terms of mean sequences, parallel sequences, horizontal branches, and O-Na anticorrelation, as shown in Figs. 3 and 4.

3.2. Differential element abundance distribution

For normalized element mass abundances $\phi_Q = Z_Q/(Z_Q)_\odot$ the empirical differential abundance distribution reads:

$$\psi_Q = \log \frac{\Delta N}{N \Delta \phi_Q} \qquad (6)$$

$$\Delta^\mp \psi_Q = \log \left[1 \mp \frac{(\Delta N)^{1/2}}{\Delta N} \right] \qquad (7)$$

where ΔN is the number of sample stars binned into $[Q/H]^\mp = [Q/H] \mp \Delta[Q/H]$, N is the sample population, and the uncertainty on ΔN, $(\Delta N)^{1/2}$, is evaluated from Poissonian errors. In addition, $\log \phi_Q = [Q/H]$ to a good extent, which implies the following:

$$\phi_Q = \frac{1}{2} \{ \exp_{10} [Q/H]^+ + \exp_{10} [Q/H]^- \} \qquad (8)$$

$$\Delta^\mp \phi_Q = \frac{1}{2} \{ \exp_{10} [Q/H]^+ - \exp_{10} [Q/H]^- \} \qquad (9)$$

where the bin $\Delta \phi_Q = \Delta^+ \phi_Q + \Delta^- \phi_Q$ is variable for fixed bin $\Delta[Q/H]$ and vice versa. For further details and complete references an interested reader is addressed to the parent papers (Caimmi 2011a, 2012a).

The empirical differential abundance distribution inferred from Eq. (6) with regard to JP12 sample, is listed in Table 3 for O, Na, Fe, where bins in $[Q/H]$ are centered on integer decibels and the bin width is $\Delta[Q/H] = 1$ dex. More specifically, $-2.6 \leq [O/H] \leq -0.7$; $-2.3 \leq [Na/H] \leq -0.9$; $-1.8 \leq [Fe/H] \leq -1.4$. The lower/upper uncertainty $\Delta^\mp \psi$ and the bin semiamplitude $\Delta^\mp \phi$ may be determined via Eqs. (7) and (9), respectively.

The results are plotted in Fig. 5 for Fe (top left panel), Na (top right panel), O (bottom right panel), all together (bottom left panel), respectively. Also, plotted on each panel is the theoretical differential abundance distribution due to cosmic scatter, assumed to obey a Gaussian distribution with parameters inferred from JP12 sample, as listed in Table 4.

Table 3. M13 empirical, differential oxygen, sodium and iron abundance distribution deduced from the JP12 sample ($N = 112$ for O and Na and $N = 113$ for Fe). The bin width in $[Q/H] = \log \phi_Q$ is $\Delta[Q/H] = 1$ dex. See text for further details.

	O		Na		Fe	
ϕ	ψ	ΔN	ψ	ΔN	ψ	ΔN
2.528552D−03	+1.187607D+00	01				
3.183258D−03	+1.388637D+00	02				
4.007485D−03		00				
5.045125D−03	+8.876073D−01	01	+8.876073D−01	01		
6.351436D−03	+7.876073D−01	01		00		
7.995984D−03	+9.886373D−01	02		00		
1.006635D−02	+1.189667D+00	04	+8.886373D−01	02		
1.267278D−02	+1.265759D+00	06	+4.876073D−01	01		
1.595408D−02	+1.232705D+00	07	+1.086577D+00	05	+3.837469D−01	01
2.008500D−02	+1.241850D+00	09	+9.865773D−01	05	+1.237989D+00	09
2.528552D−02	+1.266789D+00	12	+1.032705D+00	07	+1.996660D+00	65
3.183258D−02	+1.166789D+00	12	+1.166789D+00	12	+1.560868D+00	30
4.007485D−02	+1.266361D+00	19	+1.288637D+00	20	+8.868369D−01	08
5.045125D−02	+1.142880D+00	18	+1.091727D+00	16		
6.351436D−02	+6.906973D−01	08	+1.018056D+00	17		
7.995984D−02	+2.896673D−01	04	+8.636986D−01	15		
1.006635D−01	+1.896673D−01	04	+4.327053D−01	07		
1.267278D−01	−5.123927D−01	01	−8.966729D−02	04		
1.595408D−01		00				
2.008500D−01	−7.123927D−01	01				

Table 4. Star number N, mean abundance $\overline{[Q/H]} = <[Q/H]>$, rms error $\sigma_{[Q/H]}$, Q = O, Na, Fe, inferred from the JP12 sample for star classes defined above and below in the text.

class	N	$\overline{[O/H]}$	$\sigma_{[O/H]}$	$\overline{[Na/H]}$	$\sigma_{[Na/H]}$	$\overline{[Fe/H]}$	$\sigma_{[Fe/H]}$
N	13	−1.10	0.19	−1.77	0.25	−1.59	0.07
T	34	−1.30	0.10	−1.37	0.20	−1.60	0.06
H	64	−1.71	0.27	−1.26	0.19	−1.56	0.07
T+H	98	−1.57	0.30	−1.30	0.20	−1.57	0.07
N+T+H	111	−1.51	0.33	−1.35	0.26	−1.57	0.07
O$_-$	76	−1.59	0.28				
O$_+$	36	−1.24	0.15				
Na$_-$	33			−1.66	0.19		
Na$_+$	79			−1.22	0.12		

It can be seen that the empirical differential abundance distribution is consistent with its counterpart due to cosmic scatter for Fe, while the contrary holds for O and Na. The point out of scale corresponds to the oxygen abundance within a single star. The theoretical differential abundance distribution due to cosmic scatter for a selected element Q is explicitly expressed in Appendix A2.

Further inspection of Fig. 5 shows that the empirical differential abundance distribution looks quite similar for O and Na in the sense that, above and below a threshold, $\phi_O \overset{<}{\sim} 0.045$ or $[O/H] \leq -1.35$ (class O$_-$) and $\phi_{Na} \overset{<}{\sim} 0.037$ or $[Na/H] \leq -1.45$ (class Na$_-$), respectively, (i) the trend suddenly changes and (ii) a linear fit to the data may safely be performed. Interestingly, N stars exhibit $[O/H] > -1.35$ for 12/13 of the total and $[Na/H] < -1.45$ for 11/13 of the total. Conversely, H stars exhibit $[O/H] \leq -1.35$, but $[Na/H] > -1.45$ (class Na$_+$) holds for 55/64 of the total. Finally, T stars exhibit $[O/H] > -1.35$ (class O$_+$) and $[Na/H] < -1.45$ for 20/34 and 11/34 of the total, respectively. The whole set of results is listed in Table 5.
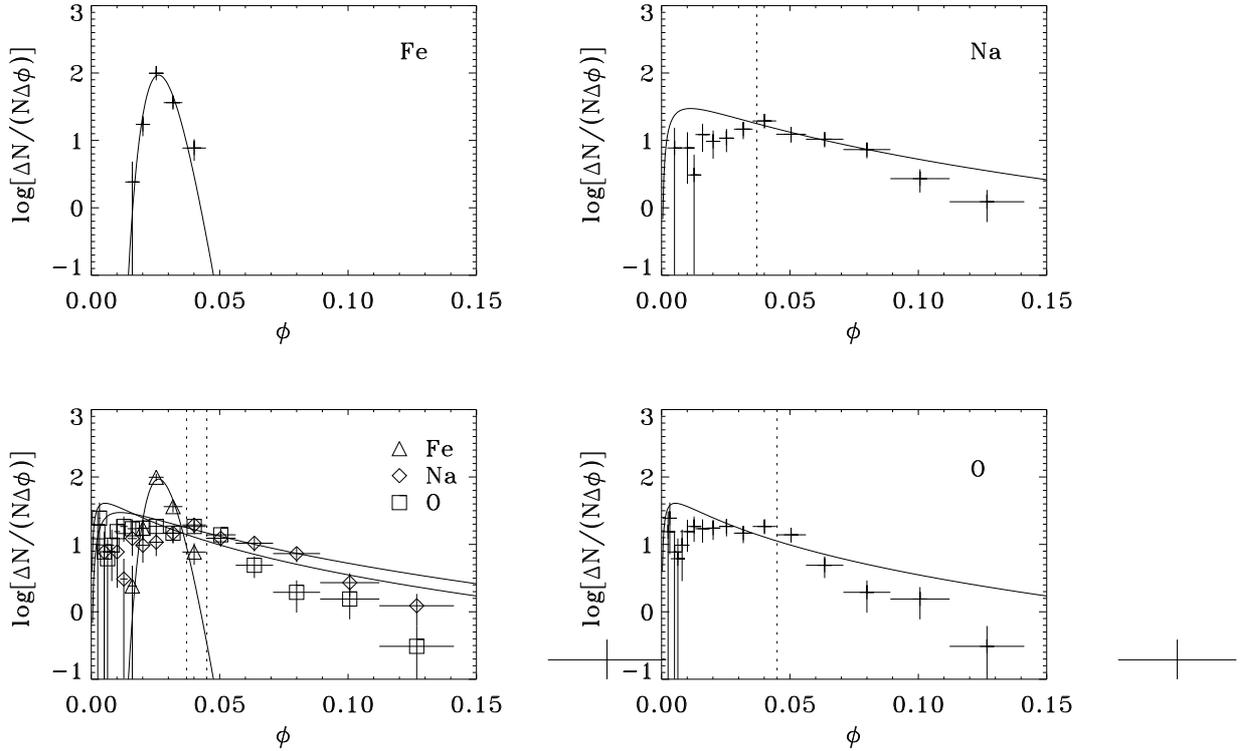
Fig. 5. *M13 empirical differential abundance distribution deduced from the JP12 sample related to Fe (top left panel), Na (top right panel), O (bottom right panel), all together (bottom left panel). The point out of scale corresponds to oxygen abundance within a single star. The theoretical differential abundance distribution due to cosmic scatter obeying a Gaussian distribution where $(x^*, \sigma_x) = (< [Q/H] >, \sigma_{[Q/H]})$, is also plotted in each panel for Fe, Na, O. The dotted vertical lines mark $\phi_O = 0.045$ or $[O/H] = -1.35$ and $\phi_{Na} = 0.037$ or $[Na/H] = -1.45$. For further details refer to the text.*

Table 5. Partition of different M13 star classes N (normal), T (transition), H (horizontal branch), into classes O_-, O_+, Na_-, Na_+, as defined in the text.

	O_-	O_+	Na_-	Na_+	all
N	1	12	11	2	13
T	14	20	11	23	34
H	64	0	9	55	64
all	79	32	31	80	111

The upper tail of the oxygen distribution $-0.9 \leq [O/H] \leq -0.7$ consists of one star per bin, for a total of two, placed at the lower boundary of the main sequence [Fe,O] plotted in Fig. 3, which might be outliers. The lower tail of the oxygen distribution $-2.6 \leq [O/H] \leq -2.2$ consists of none, one, or at most two stars per bin, for a total of five, placed at the extreme left of the horizontal branch plotted in Fig. 3, which might also be outliers.

The empirical differential abundance distribution deduced from the JP12 sample for stars belonging to class N, T, H, T + H, is listed in Tables 6 and 7 for O and Na, respectively, where bin width and uncertainties are taken as in Table 3.

The results are plotted in Figs. 6 and 7 for O (left panels) and Na (right panels).

Also plotted on each panel is the theoretical differential abundance distribution due to the cosmic scatter assumed to obey a Gaussian distribution with parameters inferred from the JP12 sample as listed in Table 4. It can be seen that the empirical differential abundance distribution is consistent with its counterpart due to cosmic scatter, to an acceptable extent for class N (O, Na), T (Na), H (Na), while the opposite holds for class T (O), H (O), T + H (O, Na).

The empirical differential abundance distribution deduced from the JP12 sample for classes O_-, O_+, and Na_-, Na_+, is listed in Table 8 second and third columns, respectively, where bin widths and uncertainties are taken as in Table 3.

Table 6. M13 empirical differential oxygen abundance distribution deduced from the JP12 sample for stars belonging to class N ($N = 13$), T ($N = 34$), H ($N = 64$), T + H ($N = 98$). See text for further details.

ϕ	class N ψ	ΔN	class T ψ	ΔN	class H ψ	ΔN	class T + H ψ	ΔN
2.53D−3					+1.43D+0	1	+1.25D+0	1
3.18D−3					+1.63D+0	2	+1.45D+0	2
4.01D−3						0		0
5.05D−3					+1.13D+0	1	+9.46D−1	1
6.35D−3					+1.03D+0	1	+8.46D−1	1
8.00D−3					+1.23D+0	2	+1.05D+0	2
1.01D−2					+1.43D+0	4	+1.25D+0	4
1.27D−2					+1.51D+0	6	+1.32D+0	6
1.60D−2					+1.48D+0	7	+1.29D+0	7
2.01D−2					+1.48D+0	9	+1.30D+0	9
2.53D−2					+1.51D+0	12	+1.32D+0	12
3.18D−2					+1.41D+0	12	+1.22D+0	12
4.01D−2	+9.23D−1	1	+1.41D+0	8	+1.08D+0	7	+1.22D+0	15
5.05D−2	+1.12D+0	2	+1.64D+0	17			+1.18D+0	17
6.35D−2	+1.20D+0	3	+1.00D+0	5			+5.45D−1	5
8.00D−2	+1.10D+0	3	+6.82D−1	3			+2.23D−1	3
1.01D−1	+8.24D−1	2	+1.05D−1	1			−3.54D−1	1
1.27D−1	−4.23D−1	1						
1.60D−1		0						
2.01D−1	−2.23D−1	1						
total		13		34		64		98

Table 7. M13 empirical differential sodium abundance distribution deduced from the JP12 sample for stars belonging to class N ($N = 13$), T ($N = 34$), H ($N = 64$) and T+H ($N = 98$). See text for further details.

ϕ	class N ψ	ΔN	class T ψ	ΔN	class H ψ	ΔN	class T + H ψ	ΔN
5.05D−3	+1.82D+0	1						
6.35D−3		0						
8.00D−3		0						
1.01D−2	+1.82D+0	2						
1.27D−2		0	+1.01D+0	1			+5.46D−01	1
1.60D−2	+2.02D+0	5		0				0
2.01D−2	+1.52D+0	2	+8.05D−1	1	+8.32D−1	2	+8.23D−01	3
2.53D−2	+1.12D+0	1	+1.40D+0	5	+4.31D−1	1	+1.02D+00	6
3.18D−2		0	+1.30D+0	5	+1.18D+0	7	+1.22D+00	12
4.01D−2	+9.23D−1	1	+1.28D+0	6	+1.34D+0	13	+1.32D+00	19
5.05D−2	+8.23D−1	1	+1.10D+0	5	+1.13D+0	10	+1.12D+00	15
6.35D−2			+1.08D+0	6	+1.07D+0	11	+1.08D+00	17
8.00D−2			+6.82D−1	3	+9.72D−1	11	+8.92D−01	14
1.01D−1			+4.06D−1	2	+5.30D−1	5	+4.91D−01	7
1.27D−1					+3.33D−1	4	+1.48D−01	4
total		13		34		64		98
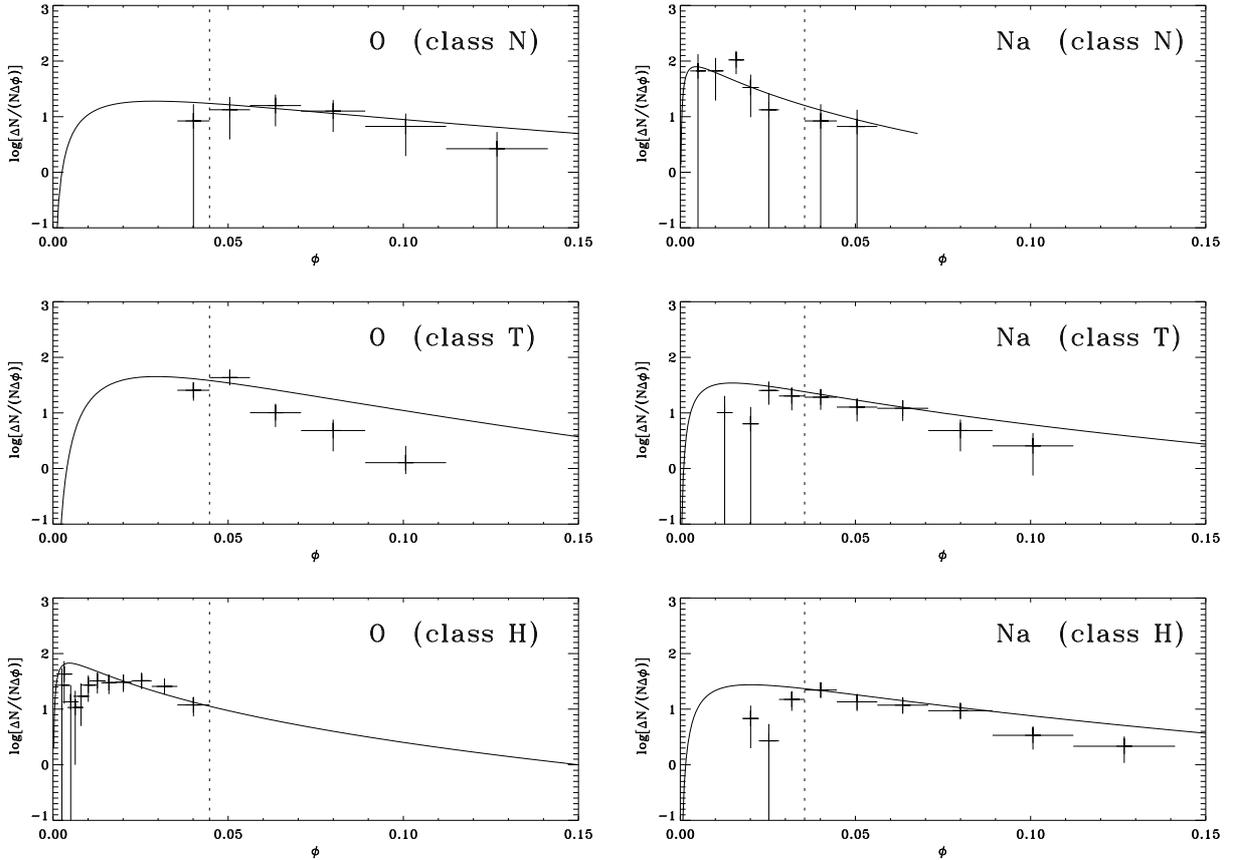
Fig. 6. *M13 empirical differential abundance distribution deduced from the JP12 sample for stars belonging to class N (N = 13), T (N = 34), H (N = 64), related to O (left panels) and Na (right panels). The theoretical differential distribution due to cosmic scatter obeying a Gaussian distribution where $(x^*, \sigma_x) = (< [Q/H] >, \sigma_{[Q/H]})$, is also plotted on each panel for O, Na. The dotted vertical lines mark $\phi_O = 0.045$ or $[O/H] = -1.35$ and $\phi_{Na} = 0.035$ or $[Na/H] = -1.45$. For further details refer to the text.*

The results are plotted in Fig. 8 together with related theoretical differential abundance distributions due to cosmic scatter, assumed to obey a Gaussian distribution with parameters inferred from the JP12 sample as listed in Table 4. It can be seen that the empirical differential abundance distribution is not consistent with its counterpart due to cosmic scatter.

The empirical differential oxygen and sodium abundance distribution, plotted in Fig. 5, is characterized by the presence of two stages exhibiting a nearly linear trend, which will be named as AF, CE, for increasing element abundance. Linear fits to each stage, $\psi = a\phi + b$, are performed using the bisector regression (Isobe et al. 1990, Caimmi 2011b, 2012b) leaving aside bins related to single stars. The regres-sion line slope and intercept estimators and related dispersion estimators are listed in Table 9 for each stage of the O and Na empirical distributions plotted in Fig. 5.

Interesting features shown in Table 9 read (i) the slope of oxygen distribution above the threshold (CE) and sodium distribution below the threshold (AF) are equal and opposite within the errors and (ii) the intercept of oxygen and sodium distribution above the threshold (CE) are equal within the errors. The regression lines are represented in Fig. 9 for each stage according to slope and intercept values listed in Table 9. To ensure continuity, AF and CE stages are bounded by the intersections of related regression lines.
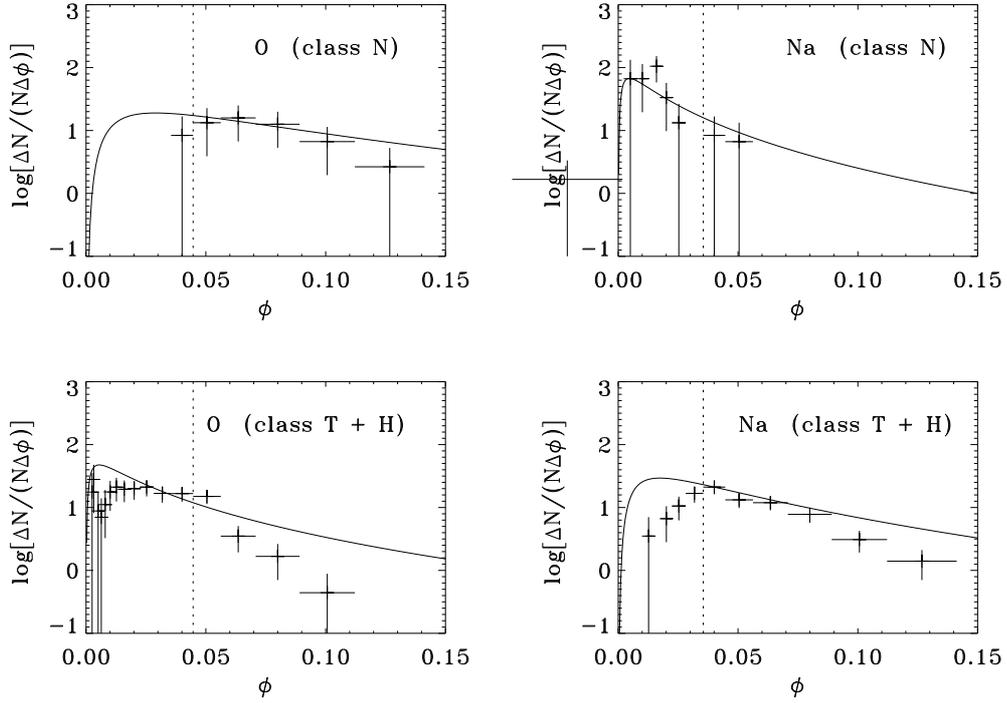
Fig. 7. *M13 empirical differential abundance distribution deduced from the JP12 sample for stars belonging to class N (N = 13; repeated for comparison), and T+H (N = 98), related to O (left panels) and Na (right panels). The point out of scale corresponds to the oxygen abundance within a single star. Other captions as in Fig. 6.*
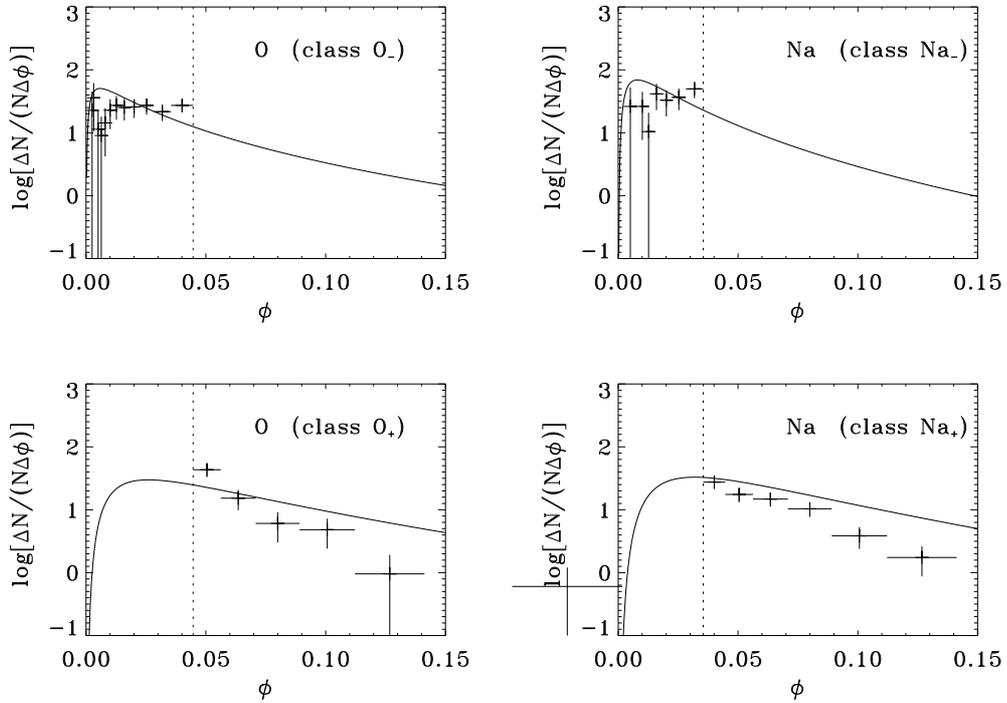
Fig. 8. *M13 empirical differential abundance distribution deduced from the JP12 sample for stars belonging to classes O_ (N = 76), O_+ (N = 36), Na_ (N = 33), Na_+ (N = 79). Other captions as in Fig. 7.*

Table 8. M13 empirical differential oxygen and sodium abundance distribution deduced from the JP12 sample for stars belonging to classes O$_-$ ($N = 36$), [O/H] ≤ -1.35 or $\phi \overset{<}{\sim} 0.040$, O$_+$ ($N = 76$), [O/H] > -1.35 or $\phi \overset{>}{\sim} 0.045$, Na$_-$ ($N = 33$), [Na/H] ≤ -1.45 or $\phi \overset{<}{\sim} 0.035$, Na$_+$ ($N = 79$), [Na/H] > -1.35 or $\phi \overset{>}{\sim} 0.035$. See text for further details.

	O		Na	
ϕ	ψ	ΔN	ψ	ΔN
2.528552D−03	+1.356012D+00	01		
3.183258D−03	+1.557042D+00	02		
4.007485D−03		00		
5.045125D−03	+1.056012D+00	01	+1.418311D+00	01
6.351436D−03	+9.560117D−01	01		00
7.995984D−03	+1.157042D+00	02		00
1.006635D−02	+1.358072D+00	04	+1.419341D+00	02
1.267278D−02	+1.434163D+00	06	+1.018311D+00	01
1.595408D−02	+1.401110D+00	07	+1.617281D+00	05
2.008500D−02	+1.410254D+00	09	+1.517281D+00	05
2.528552D−02	+1.435193D+00	12	+1.563409D+00	07
3.183258D−02	+1.335193D+00	12	+1.697493D+00	12
4.007485D−02	+1.434765D+00	19	+1.440228D+00	20
5.045125D−02	+1.635795D+00	18	+1.243318D+00	16
6.351436D−02	+1.183613D+00	08	+1.169647D+00	17
7.995984D−02	+7.825828D−01	04	+1.015289D+00	15
1.006635D−01	+6.825828D−01	04	+5.842963D−01	07
1.267278D−01	−1.947718D−02	01	+2.412582D−01	04
1.595408D−01		00		
2.008500D−01	−2.194772D−01	01		

Table 9. Regression line slope and intercept estimators $\hat{a}$ and $\hat{b}$ and related dispersion estimators $\hat{\sigma}_{\hat{a}}$, and $\hat{\sigma}_{\hat{b}}$ for regression models applied to the empirical differential oxygen and sodium abundance distribution plotted in Fig. 5, bottom and top right panels, respectively. The method has been applied to each stage (XX) separately. Data points on the boundary between AF and CE stages are used for determining regression lines within both of them. Bins containing a single star are not considered in the regression.

XX	$\hat{a}$	$\hat{\sigma}_{\hat{a}}$	$\hat{b}$	$\hat{\sigma}_{\hat{b}}$	class
AF	−1.4520 E+0	1.6466 E+0	1.2600 E+0	5.4019 E−2	O$_-$
CE	−2.0886 E+1	4.5526 E+0	2.1346 E+0	3.0319 E−1	O$_+$
AF	+1.6409 E+1	4.9000 E+0	7.2001 E−1	8.3895 E−2	Na$_-$
CE	−1.3443 E+1	1.1448 E+0	1.8272 E+0	7.0398 E−2	Na$_+$

Table 10. Transition points between adjacent stages as determined from the intersection of related regression lines for the empirical differential oxygen and sodium abundance distribution plotted in Fig. 9, top left and right panels, respectively.

transition	ϕ	ψ	Q
OO-AF	2.5286 E−3	+1.2563 E−0	O
AF-CE	4.5002 E−2	+1.1947 E−0	O
CE-OO	2.5286 E−1	−3.1465 E−0	O
OO-AF	4.4668 E−3	+7.9296 E−1	Na
AF-CE	3.7088 E−2	+1.3286 E−0	Na
CE-OO	1.4125 E−1	−7.1773 E−2	Na

The results are listed in Table 10 where OO denotes element abundance ranges without data, $0 \leq \phi \leq \phi_i$ or $\phi \geq \phi_f$, and ϕ_i and ϕ_f are the minimum and maximum element abundance, respectively, within sample stars.

Accordingly, a vertical line instead of a regression line is considered for the intersection points related to OO-AF and CE-OO transitions.
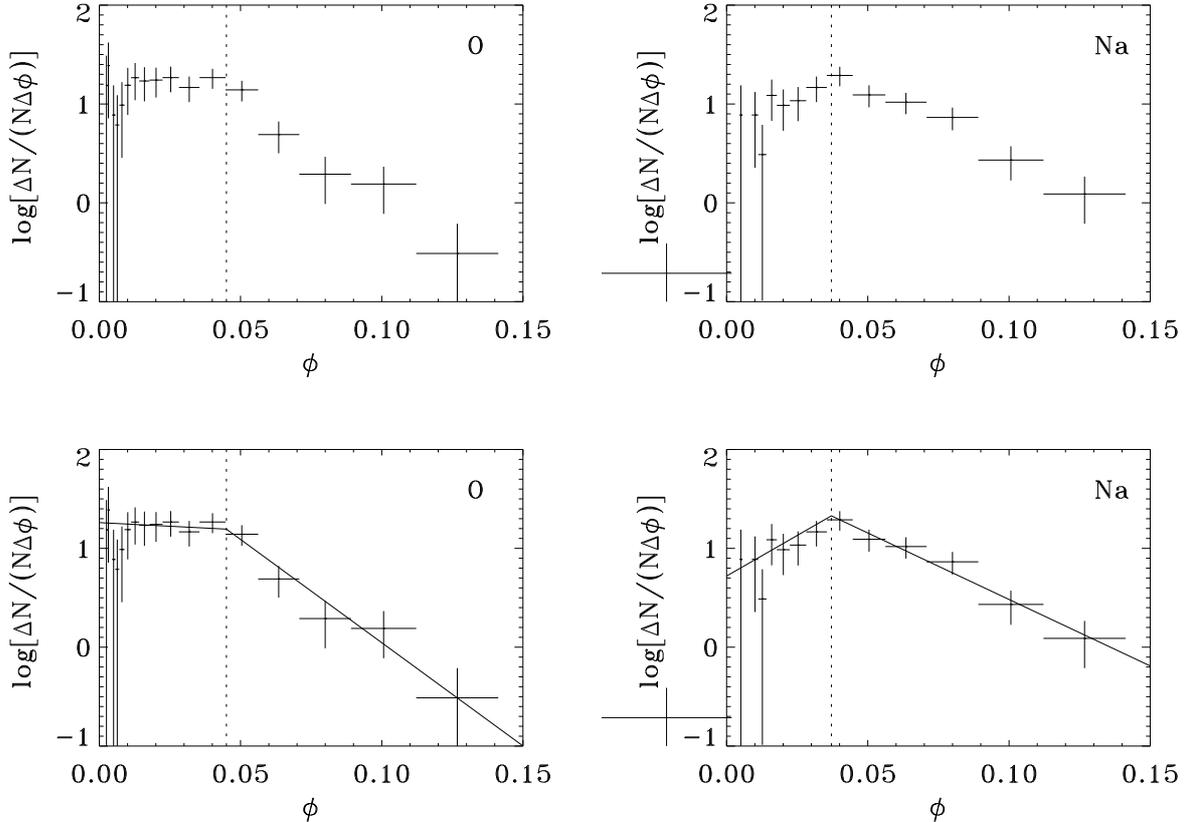
Fig. 9. *Regression lines to the empirical differential oxygen (top left) and sodium (top right) abundance distributions listed in Table 3 with regard to stages (from the left to the right) AF and CE. Bins containing a single star are not used for the regression. The abscissa of the intersection point of regression lines is marked by a dashed vertical line. Other captions as in Fig. 5. For further details refer to the text.*

4. DISCUSSION

The GC star classification defined in Section 2 is rigorous and well motivated in that it relates to the main sequence defined by field halo stars, as shown in Figs. 3 and 4 in the case under consideration of M13. The validity of the proposed classification may be tested in a twofold manner, namely, by extending Figs. 3 and 4 to (i) elements other than Na, Fe, and (ii) GCs other than M13. In any case, the expected trend implies part of sample stars within the above mentioned main sequence, part on a horizontal branch (Fig. 3) or, in addition, on one or more parallel sequences towards lower oxygen abundance (Fig. 4). For a given element, different GCs are expected to depart from the main sequence at different points, depending on their primordial abundance in that element.

Caution is needed in the interpretation of quantitative results owing to currently large abundance mesaurement errors for GC stars (e.g. Renzini 2013). Let the trend exhibited by element abundance

remain only slightly affected even if the uncertainty on single stars is high, typically ∓ 1.5 dex for M13 (JP12). Under this assumption, valuable informations can be extracted from the empirical differential element abundance distribution, as shown in Fig. 9 for M13, where a threshold is clearly exhibited at $[O/H] \approx -1.35$ and $[Na/H] \approx -1.45$, respectively. More specifically, different slopes in different regions could reflect the occurrence of different physical processes during the evolution.

An inspection of Table 5 shows the whole sample of H stars is depleted in oxygen, $[O/H] \leq -1.35$ (class O_-), while 55/64 of the total are enriched in sodium, $[Na/H] > -1.45$ (class Na_+), which might be interpreted in a twofold manner: either the sodium enrichment is not the sole channel of oxygen depletion, or sodium is, in turn, partially depleted. In fact, the empirical differential sodium abundance distribution for classes N, T, H, is consistent, to an acceptable extent, with its theoretical counterpart due to intrinsic scatter, leaving aside a few sodium-deficient stars, as shown in Fig. 6. With regard to oxygen, a similar trend is exhibited for class N, while the

contrary holds for classes T, H. The above results are consistent with little or no chemical evolution for oxygen within class N and sodium within classes N, T, H. On the other hand, the oxygen chemical evolution did take place, even if partially, within classes T, H, and, in any case, passing from O_+ to O_- class and from Na_- to Na_+ class.

To this respect, the simplest assumption is a constant yield for both oxygen and sodium, in the light of simple MCBR (multistage closed box + reservoir) models of chemical evolution (Caimmi 2011a, 2012a) where gas inflow and outflow are allowed. In the special case of a linear fit to the empirical differential abundance distribution:

$$\psi_Q = a_Q \phi_Q + b_Q \qquad (10)$$

the slope has the explicit expression:

$$a_Q = -\frac{1}{\ln 10} \frac{(Z_Q)_\odot}{\hat{p}_Q} (1 + \kappa) \qquad (11)$$

where Q = O, Na, and κ is the flow parameter, positive for outflow and negative for inflow. For further details an interested reader is addressed to the parent papers (Caimmi 2011a, 2012a).

The oxygen-to-sodium yield ratio, inferred from Eq. (11), reads:

$$\frac{\hat{p}_O}{\hat{p}_{Na}} = \frac{a_{Na}}{a_O} \frac{(Z_O)_\odot}{(Z_{Na})_\odot} \qquad (12)$$

where the slope ratio a_{Na}/a_O has necessarily to be negative for O depletion and Na enrichment, which implies an opposite sign for slopes related to classes O_-, Na_+, and O_+, Na_-, listed in Table 10. Accordingly, the slope related to class O_-, within the errors, restricts to $0 < a_O \le 0.1946$. Then $a_{Na}/a_O = -1$ for stars belonging to classes O_+ and Na_-, within the errors, while $a_{Na}/a_O \overset{<}{\sim} -69$ for stars belonging to classes O_- and Na_+.

The substitution of the above mentioned values into Eq. (12) yields:

$$\frac{\hat{p}_O}{\hat{p}_{Na}} = -\frac{(Z_O)_\odot}{(Z_{Na})_\odot} \qquad (13)$$

in the former alternative and

$$\frac{\hat{p}_O}{\hat{p}_{Na}} \overset{<}{\sim} -69 \frac{(Z_O)_\odot}{(Z_{Na})_\odot} \qquad (14)$$

in the latter alternative. According to Eq. (13), O depletion can be entirely turned into Na enrichment during the early evolution ([O/H] ≥ -1.35, [Na/H] ≤ -1.45). Conversely, according to Eq. (14), O depletion appears to be mainly turned into Q

other than Na enrichment during the late evolution ([O/H] < -1.35, [Na/H] > -1.45).

As an exercise, let the sodium chemical evolution in M13 be considered within the framework of simple MCBR models in the linear limit (Caimmi 2011a, 2012a). Sodium may be conceived as a primary element provided it is synthesised mainly from oxygen which is, in turn, a primary element. Accordingly, the following relations hold together with Eqs. (10)-(12):

$$\frac{\mu_f}{\mu_i} = \exp_{10} \left\{ a_Q \left[(\phi_Q)_f - (\phi_Q)_i \right] \right\} \qquad (15)$$

$$s_f - s_i = \frac{\mu_i}{1 + \kappa} \left(1 - \frac{\mu_f}{\mu_i} \right) \qquad (16)$$

$$D_f - D_i = \kappa (s_f - s_i) \qquad (17)$$

$$\zeta_Q = 1 - \frac{A_Q \hat{p}_Q}{\kappa} \qquad (18)$$

where μ is the gas mass fraction, s the long-lived star mass fraction, D the flowing gas mass fraction, ζ the ratio of Q abundance within the flowing gas to Q abundance within the pre existing gas, A_Q a coefficient which may safely be expressed as $A_Q = 2(Z_O)_\odot/(Z_Q)_\odot$, Q = Na in the case under discussion and the indices, i, f, denote initial and final values, respectively, with regard to the stage considered. The free parameter is chosen to be the true sodium yield $\hat{p}_{Na}$.

The cut parameter ζ_{Na}, the flow parameter κ, the active (i.e. available for star formation) gas mass fraction μ_f, the long-lived star mass fraction s_f, the flowing gas mass fraction D_f, determined in the linear limit for a true sodium yield in solar sodium abundance units, $\hat{p}_{Na}/(Z_{Na})_\odot = 0.5, 1.0, 2.0$, are listed in Table 11.

The parameters κ, D_f, are negative for inflow and positive for outflow, respectively. For each case, upper lines correspond to Na_- class ([Na/H] ≤ -1.45; AF stage) and lower lines to Na_+ class ([Na/H] > -1.45; CE stage).

Solar abundances are inferred from recent data (Asplund et al. 2009) as $(Z_{Na})_\odot = 2.950 \times 10^{-5}$ and $(Z_O)_\odot = 5.786 \times 10^{-3}$ (Caimmi 2013). The initial values at the AF stage are chosen as $\mu_i = 1$; $s_i = 0$; $D_i = 0$; accordingly, μ_f is independent of $\hat{p}_{Na}/(Z_{Na})_\odot$ via Eq. (15) and the ratio $(s_f)_{CE}/(s_f)_{AF}$ is independent of $\hat{p}_{Na}/(Z_{Na})_\odot$ via Eq. (16). If $(s_f)_{CE}$ and $(\mu_f)_{AF} + (s_f)_{AF}$ relate to the current and the primordial M13 mass, respectively, an inspection of Table 12 shows the primordial to current mass ratio amounts to about 10, 20, 40 for $\hat{p}_{Na}/(Z_{Na})_\odot = 0.5, 1.0, 2.0$, respectively, according to Eqs. (15)-(16). Then the M13 primordial mass can be inferred within the framework of the model, from the knowledge of the true sodium yield.

Table 11. Values of the cut parameter ζ_{Na}, the flow parameter κ, the active gas mass fraction μ_f, the long-lived star mass fraction s_f, the flowing gas mass fraction D_f, for different values of the true sodium yield in solar sodium abundance units, $\hat{p}_{\mathrm{Na}}/(Z_{\mathrm{Na}})_\odot$, in the linear limit. For each case, upper lines correspond to Na_- class ($[\mathrm{Na/H}] \leq -1.45$; AF stage) and lower lines to Na_+ class ($[\mathrm{Na/H}] > -1.45$; CE stage). For further details refer to the text.

$\hat{p}_{\mathrm{Na}}/(Z_{\mathrm{Na}})_\odot$	ζ_{Na}	κ	μ_f	s_f	D_f	XX	class
0.5	1.0003E$-$0	$-$1.9893E$+$1	3.4302E$-$0	1.2863E$-$1	$-$2.5588E$-$0	AF	Na_-
	9.9960E$-$1	$+$1.4477E$+$1	1.3648E$-$1	3.4144E$-$1	$+$5.2208E$-$1	CE	Na_+
1.0	1.0003E$-$0	$-$3.8786E$+$1	3.4302E$-$0	6.4315E$-$2	$-$2.4945E$-$0	AF	Na_-
	9.9961E$-$1	$+$2.9954E$+$1	1.3648E$-$1	1.7072E$-$1	$+$6.9280E$-$1	CE	Na_+
2.0	1.0003E$-$0	$-$7.6571E$+$1	3.4302E$-$0	3.2157E$-$2	$-$2.4623E$-$0	AF	Na_-
	9.9962E$-$1	$+$6.0907E$+$1	1.3648E$-$1	8.5361E$-$2	$+$7.7816E$-$1	CE	Na_+

5. CONCLUSION

The main results of the current paper may be summarized as follows.

(1) Based on the "main sequence" defined by halo and thick disk low-metallicity ([Fe/H] < -0.6) stars on the (O[O/H][Q/H]) plane (Caimmi 2013), a natural and well motivated selection criterion has been defined for classifying GC stars with respect to a selected element Q, and to oxygen O.

(2) An application has been performed to M13 using a star sample ($N = 113$) for which O, Na, Fe abundance is available (JP12): previously classified primordial stars are found to lie (leaving aside two exceptions) within the above mentioned main sequence (class N); previously classified intermediate stars are found to lie (in comparable amount) within both a parallel main sequence (towards lower [O/H]; class T) and a "horizontal branch" (class H); previously classified extreme stars are found to lie within the above mentioned horizontal branch; as shown in Table 2 and in Figs. 3, 4.

(3) Both O and Na empirical differential abundance distributions have been determined for each class and the whole sample (with the addition of Fe in the last case) and compared with their theoretical counterparts due to cosmic scatter obeying a Gaussian distribution whose parameters were inferred from related subsamples. For the whole sample, an acceptable fit has been found only for Fe, as shown in Fig. 5, which has been extended to class N for both O and Na and to class T and H for Na with the exception of a few sodium-deficient stars, as shown in Fig. 6. No fit occurs for

T + H class and for stars where [O/H]$<$ -1.35 (class O$_-$), [O/H]≥ -1.35 (class O$_+$), [Na/H]≤ -1.45 (class Na$_-$), [Na/H]> -1.45 (class Na$_+$), as shown in Figs. 7, 8, which has been interpreted as a signature of chemical evolution.

(4) Both empirical O and Na differential abundance distributions, related to the whole sample, have been fitted by a straight line with regard to O$_-$, O$_+$, Na$_-$, Na$_+$ classes, respectively, where the slopes related to O$_+$ and Na$_-$ classes were equal and opposite in sign within the errors, while the contrary was found for O$_-$ and Na$_+$ classes, as shown in Table 10 and in Fig. 9. The above results have been interpreted as consistent with the oxygen depletion mainly turned into sodium enrichment for [O/H]≥ -1.35, [Na/H]≤ -1.45, and implying oxygen depletion through most preferred channels with respect to Na for [O/H]< -1.35, [Na/H]> -1.45.

(5) In the light of the simple MCBR models of chemical evolution in the linear limit, the ratio of M13 primordial to current mass has been found to be proportional to the true sodium yield in units of sodium solar abundance, as shown in Table 12, where $M_{\mathrm{primordial}}/M_{\mathrm{current}} = [(\mu_f)_{\mathrm{AF}} + (s_f)_{\mathrm{AF}}]/(s_f)_{\mathrm{CE}}$.

As current abundance determinations, [Q/H], are affected by large (∓ 1.5 dex) uncertainties in GC stars, the above results are to be considered as mainly qualitative but the trends shown are expected to be real. As already mentioned in Section 4, the validity of the proposed classification may be tested in a twofold manner, namely, by extending Figs. 3 and 4 to (i) elements other than Na, Fe, and (ii) GCs other than M13.

REFERENCES

Asplund, M., Grevesse, N., Sauval, A. J., Scott, P.: 2009, *Annu. Rev. Astron. Astrophys.*, **47**, 481.

Caimmi, R.: 2011a, *Serb. Astron. J.*, **183**, 37.

Caimmi, R.: 2011b, *New Astron.*, **16**, 337.

Caimmi, R.: 2012a, *Serb. Astron. J.*, **185**, 85.

Caimmi, R.: 2012b, *Intellectual Archive*, **1**, 71, (arXiv:1111.2680)

Caimmi, R.: 2013, arXiv:1306.6750.

Caimmi, R., Milanese, E.: 2009, *Astrophys. Space Sci.*, **323**, 147.

Carretta, E., Bragaglia, A., Gratton, R., Lucatello, S.: 2009a, *Astron. Astrophys.*, **505**, 139.

Carretta, E., Bragaglia, A., Gratton, R. G., et al.: 2009b, *Astron. Astrophys.*, **505**, 117.

Cassisi, S., Salaris, M., Pietrinferni, A.: 2013, *Mem. S. A. It.*, **84**, 91. (arXiv:1212.6839)

Conroy, C.: 2012, *Astrophys. J.*, **758**, 21. (C12)

Gratton, R. G., Carretta, E., Bragaglia, A.: 2012. *Astron. Astrophys. Rew.*, **20**, 50.

Isobe, T., Feigelson, E. D., Akritas, M. G., Babu, G. J.: 1990, *Astrophys. J.*, **364**, 104.

Johnson, C. I., Pilachowski, C. A., 2012. *Astrophys. J.*, **754**, L38. (JP12)

Nissen, P. E., Schuster, W. J., 2010. *Astron. Astrophys.*, **511**, L10. (NS10)

Piotto, G.: 2009, in Proc. IAU Symposium 258, ed. E. E. Mamajek, D. R. Söderblom, and R.F.G. Wyse, Cambridge University Press, Cambridge, 233.

Ramirez, I., Melendez, J., Chanamé, J.: 2012, *Astrophys. J.*, **757**, 164. (Ra12)

Renzini, A.: 2013, *Mem. S. A. It.*, **84**, 162. (arXiv:1302.0329)

Ventura, P., Di Criscienzo, M., Carini, R., D'Antona, F.: 2013, *Mon. Not. R. Astron. Soc.*, **431**, 3642.

APPENDIX

A1 JP12 sample star data

The whole set of JP12 sample star data used in the current attempt is listed in Table 12 where the following denomination or value appears in each column: (1) star name; (2) other star name; (3) [O/H]; (4) [Fe/H]; (5) [Na/H]; (6) b_{Fe} via Eq. (1) where $a_{Fe} = 1.00$; (7) b_{Na} via Eq. (1) where $a_{Na} = 1.25$; (8) population (P, I, E) as defined in the parent paper (JP12); (9) Fe class according to Eq. (3); (10) Na class according to Eq. (4); (11) Fe-Na class (N, T, H) according to Eqs. (5).

Table 12. M13 star classification according to the parent paper (JP12) and the current attempt. Number abundances [O/H], [Fe/H], [Na/H] are taken or inferred from the parent paper. Intercepts b_Q relate to the straight line $[Q/H] = a_Q[O/H] + b_Q$ passing through the point $([Q/H],[O/H])$ where Q = Fe, Na, $a_{Fe} = 1.00$, $a_{Na} = 1.25$. Population P (primitive), I (intermediate), E (extreme), are defined as in the parent paper. Classes with different degree of anomaly A_i, $i = 0, \mp1, \mp2, ...$, with regard to Q = Fe, Na, are defined as in the text. Class A_{-1} is listed as $-A_1$ for the sake of aesthetics. Classes N (normal), T (transition), H (horizontal branch), are defined as in the text. See text for further details.

name	other	[O/H]	[Fe/H]	[Na/H]	b_{Fe}	b_{Na}	p	Fe	Na	c
L 324	V11	−1.96	−1.50	−1.23	0.46	1.22	E	A_2	A_3	H
L 598	...	−1.35	−1.44	−1.58	−0.09	0.11	P	A_1	A_1	H
L 629	...	−1.63	−1.57	−1.37	0.06	0.67	I	A_1	A_2	H
L 194	II-90	−1.90	−1.49	−1.13	0.41	1.25	E	A_2	A_3	H
L 973	I-48	−2.55	−1.50	−1.23	1.05	1.96	E	A_3	A_4	H
L 835	V15	−2.16	−1.50	−1.10	0.66	1.60	E	A_2	A_3	H
L 954	IV-25	−2.00	−1.48	−1.12	0.52	1.38	E	A_2	A_3	H
L 940	...	−2.09	−1.53	−1.36	0.56	1.25	E	A_2	A_3	H
L 70	II-67	−2.45	−1.45	−1.12	1.00	1.94	E	A_3	A_4	H
L 199	III-63	−1.51	−1.61	−1.41	−0.10	0.48	I	A_1	A_1	H
L 853	...	−1.50	−1.51	−1.31	−0.01	0.57	I	A_1	A_2	H
L 261	...	−1.59	−1.59	−1.53	0.00	0.46	I	A_1	A_1	H
L 262	...	−1.52	−1.58	−1.36	−0.06	0.54	I	A_1	A_2	H
L 72	III-73	−1.45	−1.59	−1.75	−0.14	0.06	P	A_1	A_1	H
L 240	II-34	−1.82	−1.42	−1.12	0.40	1.16	E	A_2	A_3	H
L 481	...	−2.26	−1.49	−1.12	0.77	1.71	E	A_2	A_4	H
L 250	...	−1.86	−1.58	−1.20	0.28	1.12	E	A_1	A_3	H
L 384	...	−1.25	−1.61	−1.57	−0.36	−0.01	I	A_0	A_1	T

Table 12. Continued.

name	other	[O/H]	[Fe/H]	[Na/H]	b_{Fe}	b_{Na}	p	Fe	Na	c
L 465	...	-1.26	-1.64	-1.79	-0.38	-0.21	P	A_0	A_0	N
L 96	II-76	-1.20	-1.63	-1.72	-0.43	-0.22	P	A_0	A_0	N
L 845	...	-2.05	-1.57	-1.17	0.48	1.39	E	A_2	A_3	H
L 745	I-13	-1.35	-1.55	-1.91	-0.20	-0.22	P	A_1	A_0	T
L 584	...	-1.40	-1.63	-1.95	-0.23	-0.20	I	A_0	A_0	N
L 296	...	-1.45	-1.71	-1.43	-0.26	0.38	I	A_0	A_1	T
L 367	...	-2.01	-1.57	-1.17	0.44	1.34	E	A_2	A_3	H
L 316	III-59	-1.80	-1.62	-1.38	0.18	0.87	E	A_1	A_2	H
L 549	...	-1.35	-1.62	-1.18	-0.27	0.51	I	A_0	A_2	T
L 674	...	-1.61	-1.62	-1.18	-0.01	0.83	I	A_1	A_2	H
L 398	...	-1.30	-1.55	-1.47	-0.25	0.16	I	A_0	A_1	T
L 244	III-52	-1.70	-1.62	-1.36	0.08	0.77	I	A_1	A_2	H
L 252	II-33	-1.38	-1.60	-1.58	-0.22	0.15	I	A_0	A_1	T
L 830	...	-1.91	-1.59	-1.07	0.32	1.32	E	A_2	A_3	H
L 938	IV-53	-1.17	-1.63	-1.21	-0.46	0.25	P	A_0	A_1	T
L 158	II-57	-1.80	-1.58	-1.52	0.22	0.73	E	A_1	A_2	H
L 666	...	-1.30	-1.57	-1.45	-0.27	0.17	I	A_0	A_1	T
L 77	III-18	-1.86	-1.62	-1.18	0.24	1.14	E	A_1	A_3	H
L 169	III-37	-1.86	-1.52	-1.03	0.34	1.29	E	A_2	A_3	H
L 825	...	-1.61	-1.55	-1.12	0.06	0.89	I	A_1	A_2	H
L 353	II-40	-1.23	-1.58	-1.81	-0.35	-0.27	P	A_0	A_0	N
L 594	...	-1.45	-1.57	-1.12	-0.12	0.69	I	A_1	A_2	H
L 777	I-24	-1.37	-1.57	-1.43	-0.20	0.28	I	A_1	A_1	H
L 1073	...	-1.32	-1.64	-1.58	-0.32	0.07	I	A_0	A_1	T
L 754	...	-1.26	-1.60	-1.51	-0.34	0.07	I	A_0	A_1	T
L 198	...	-1.51	-1.53	-1.06	-0.02	0.83	I	A_1	A_2	H
L 687	IV-15	-1.55	-1.65	-1.52	-0.10	0.42	I	A_1	A_1	H
L 863	I-42	-1.70	-1.59	-1.48	0.11	0.64	I	A_1	A_2	H
L 1023	IV-61	-1.71	-1.50	-1.19	0.21	0.95	E	A_1	A_2	H
L 877	I-50	-1.45	-1.66	-1.29	-0.21	0.52	I	A_0	A_2	T
L 919	IV-28	-1.75	-1.62	-1.27	0.13	0.92	I	A_1	A_2	H
K 656	...	-1.31	-1.57	-1.54	-0.26	0.10	I	A_0	A_1	T
L 343	...	-1.25	-1.60	-1.41	-0.35	0.15	I	A_0	A_1	T
L 592	...	-1.40	-1.68	-1.37	-0.28	0.38	I	A_0	A_1	T
L 476	...	-1.32	-1.62	-1.40	-0.30	0.25	I	A_0	A_1	T
L 269	...	-1.76	-1.65	-1.44	0.11	0.76	I	A_1	A_2	H
L 948	IV-35	-1.39	-1.64	-1.46	-0.25	0.28	I	A_0	A_1	T
L 967	I-86	-2.01	-1.55	-1.17	0.46	1.34	E	A_2	A_3	H
L 1030	I-77	-1.30	-1.61	-1.46	-0.31	0.17	I	A_0	A_1	T
L 644	...	-1.66	-1.62	-1.30	0.04	0.78	I	A_1	A_2	H
L 773	I-23	-1.35	-1.66	-1.32	-0.31	0.37	I	A_0	A_1	T
L 956	...	-1.45	-1.63	-1.26	-0.18	0.55	I	A_1	A_2	H
K 228	J 3	-1.51	-1.45	-0.93	0.06	0.96	I	A_1	A_2	H
L 176	II-87	-1.40	-1.61	-1.24	-0.21	0.51	I	A_0	A_2	T
K 188	A1	-1.15	-1.52	-1.30	-0.37	0.14	I	A_0	A_1	T
L 436	...	-1.70	-1.78	-1.42	-0.08	0.70	I	A_1	A_2	H
L 114	III-7	-1.45	-1.61	-1.26	-0.16	0.55	I	A_1	A_2	H
L 370	...	-1.85	-1.66	-1.39	0.19	0.92	E	A_1	A_2	H
L 1043	BAUM13	-1.43	-1.67	-1.10	-0.24	0.69	I	A_0	A_2	T
L 766	I-12	-1.65	-1.63	-1.43	0.02	0.63	I	A_1	A_2	H
L 172	III-45	-1.40	-1.58	-1.41	-0.18	0.34	I	A_1	A_1	H

Table 12. Continued.

name	other	[O/H]	[Fe/H]	[Na/H]	b_{Fe}	b_{Na}	p	Fe	Na	c
L 26	J38	-1.65	-1.51	-1.23	0.14	0.83	I	A_1	A_2	H
L 168	II-28	-1.03	-1.64	-2.30	-0.61	-1.01	P	A_0	$-A_1$	N
L 193	II-94	-1.60	-1.56	-1.01	0.04	0.99	I	A_1	A_2	H
L 726	IV-19	-1.28	-1.54	-1.38	-0.26	0.22	I	A_0	A_1	T
L 793	...	-1.05	-1.59	-1.72	-0.54	-0.41	P	A_0	A_0	N
K 699	X 24	-1.38	-1.60	-1.20	-0.22	0.53	I	A_0	A_2	T
L 677	IV-4	-1.65	-1.59	-0.88	0.06	1.18	I	A_1	A_3	H
L 18	...	-1.55	-1.65	-1.54	-0.10	0.40	I	A_1	A_1	H
L 800	IV-18	-1.30	-1.59	-1.35	-0.29	0.27	I	A_0	A_1	T
L 1032	I-76	-1.40	-1.59	-1.67	-0.19	0.08	E	A_1	A_1	H
L 871	I-19	-2.46	-1.62	-0.99	0.84	2.09	E	A_3	A_4	H
L 955	IV-22	-1.45	-1.54	-1.25	-0.09	0.56	I	A_1	A_2	H
L 609	...	-1.30	-1.69	-1.22	-0.39	0.41	I	A_0	A_1	T
L 81	II-23	-1.58	-1.60	-1.04	-0.02	0.93	I	A_1	A_2	H
L 1001	I-49	-1.30	-1.54	-1.60	-0.24	0.02	P	A_0	A_1	T
K 422	...	-1.10	-1.54	-1.32	-0.44	0.05	I	A_0	A_1	T
L 1060	I-65	-1.65	-1.57	-1.36	0.08	0.70	I	A_1	A_2	H
L 162	III-43	-1.56	-1.48	-1.40	0.08	0.55	I	A_1	A_2	H
L 488	...	-1.35	-1.55	-1.30	-0.20	0.39	I	A_1	A_1	H
L 1051	IV-78	-1.86	-1.57	-1.20	0.29	1.12	E	A_1	A_3	H
L 1114	...	-1.35	-1.65	-1.64	-0.30	0.05	I	A_0	A_1	T
L 557	...	-1.13	-1.58	-1.79	-0.45	-0.38	P	A_0	A_0	N
L 79	...	-1.00	-1.55	-1.81	-0.55	-0.56	P	A_0	A_0	N
K 659	...	-1.40	-1.39	-1.06	0.01	0.69	I	A_1	A_2	H
L 140	III-25	-1.50	-1.61	-1.00	-0.11	0.88	I	A_1	A_2	H
K 674	...	-0.90	-1.59	-1.33	-0.69	-0.20	I	A_0	A_0	N
L 787	I-2	-1.28	-1.58	-1.11	-0.30	0.49	I	A_0	A_1	T
L 1050	...	-1.40	-1.47	.....	-0.07	....	.	A_1	...	.
L 1072	IV-80	-1.45	-1.55	-0.91	-0.10	0.90	I	A_1	A_2	H
L 423	II-7	-1.00	-1.51	-1.62	-0.51	-0.37	P	A_0	A_0	N
L 824	I-39	-1.25	-1.56	-1.19	-0.31	0.37	I	A_0	A_1	T
L 1096	I-67	-1.65	-1.58	-1.25	0.07	0.81	I	A_1	A_2	H
L 1097	...	-1.80	-1.48	-1.28	0.32	0.97	E	A_2	A_2	H
L 29	II-63	.....	-1.59	-1.07	.....	....	.	...	...	.
K 224	J 37	-1.15	-1.53	-1.03	-0.38	0.41	I	A_0	A_1	T
L 137	...	-1.25	-1.47	-1.07	-0.22	0.49	I	A_0	A_1	T
L 16	J50	-1.17	-1.61	-1.79	-0.44	-0.33	P	A_0	A_0	N
K 647	...	-1.65	-1.58	-1.51	0.07	0.55	I	A_1	A_2	H
L 93	III-40	-1.00	-1.42	-1.03	-0.42	0.22	I	A_0	A_1	T
L 1095	I-69	-1.30	-1.62	-1.68	-0.32	-0.05	P	A_0	A_1	T
L 6	J11	-1.70	-1.68	-1.32	0.02	0.81	I	A_1	A_2	H
L 101	II-60	-1.28	-1.68	-2.00	-0.40	-0.40	P	A_0	A_0	N
L 32	II-64	-1.43	-1.44	-0.94	-0.01	0.85	I	A_1	A_2	H
CM 12	...	-0.65	-1.39	-1.40	-0.74	-0.59	P	$-A_1$	A_0	N

A2 Differential element abundance distribution due to cosmic scatter

Let a sample be composed of N long-lived coeval stars belonging to the same generation where the abundance of the primordial gas was affected by a cosmic scatter. Let the related distribution be Gaussian in [Q/H] with respect to a selected element Q and normalized to the sample population N. The explicit expression reads:

$$\frac{dN}{N} = \frac{1}{\sqrt{2\pi}\sigma} \exp\left(-\frac{x^2}{2\sigma^2}\right) dx \qquad (19)$$

$$x = [Q/H] - \ <[Q/H]> \qquad (20)$$

where dN is the expected star number within a bin, centered on x, of infinitesimal width dx.

Keeping in mind that [Q/H]$= \log \phi_Q$ to a good extent (e.g. Caimmi 2011a), the infinitesimal bin width reads:

$$dx = d[Q/H] = \frac{1}{\ln 10} \frac{d\phi_Q}{\phi_Q} \qquad (21)$$

which is equivalent to:

$$\frac{dx}{d\phi_Q} = \frac{1}{\ln 10} \frac{1}{\phi_Q} \qquad (22)$$

according to Eq. (20).

The theoretical differential element abundance distribution due to cosmic scatter is inferred from the theoretical counterpart of Eq. (6):

$$\psi_Q = \log \frac{dN}{N \, d\phi_Q} \qquad (23)$$

after substitution of Eqs. (19) and (22) into (23). The result is:

$$(\psi_Q)_{cs} = \log \left\{ \frac{1}{\ln 10} \frac{1}{\sqrt{2\pi}\sigma} \right.$$
$$\left. \times \exp\left[-\frac{(\log \phi_Q - \overline{\log \phi_Q})^2}{2\sigma^2} \right] \frac{1}{\phi_Q} \right\} \qquad (24)$$

where cs denotes cosmic scatter and $\overline{\log \phi_Q} = \ <[Q/H]>$.

КЛАСИФИКАЦИЈА ЗВЕЗДА ЗБИЈЕНИХ ЈАТА: ПРИМЕНА НА М13

R. Caimmi

Dipartimento di Fisica e Astronomia, Università di Padova
Vicolo Osservatorio 3/2, I-35122 Padova, Italy

E–mail: *roberto.caimmi@unipd.it*

Полазећи од скорашњег одређивања садржаја Fe, O, Na на једном ограниченом узорку (N = 67) звезда халоа и дебелог диска дефинише се један природан и добро мотивисан критеријум одабира намењен класификацији звезда из збијених јата. Он се овде примењује на М13 користећи узорак (N = 113) звезда за које су садржаји Fe, O, Na недавно утврђени из посматрања. Начињено је поређење између садашње и раније класификације звезда М13. И за O и за Na емпиријске диференцијалне расподеле садржаја су одређене за сваку класу, заједно са целим узорком (укључујући и Fe у другом случају). Следи поређење са одговарајућим теоријским расподелама где имамо космичко растурање по Гаусовој расподели чији се параметри налазе из одговарајућих подузорака. Слагање између емпиријске и теоријске расподеле се тумачи као одсуство знатније хемијске еволуције и обрнуто. Поступак се понавља са четири додатне класе према томе да ли су садржаји кисеоника и натријума изнад (стадијум CE) или испод (стадијум AF) неког одабраног прага. Емпиријске диференцијалне расподеле садржаја и за O и за Na за цео узорак показују линеарни тренд за стадијуме AF и CE. Унутар граница грешке, коефицијент правца за кисеоник за стадијум CE једнак је, али супротног знака, у поређењу са истим за натријум за стадијум AF, док обрнуто важи за коефицијент правца код кисеоника за стадијум AF и коефицијент правца код натријума за стадијум CE. У светлу једноставних модела хемијске еволуције примењених на М13 смањење садржаја кисеоника углавном прелази у обогаћивање код натријума за [O/H]≥ -1.35 и [Na/H]≤ -1.45 док имамо један или више привилегованих канала за [O/H]< -1.35 и [Na/H]> -1.45. Осим тога, однос првобитне и садашње масе за М13 може да се установи из стварног стварања натријума у јединицама удела натријума код Сунца. Премда су горњи резултати углавном квалитативни услед великих грешака (∓ 1.5 dex) одређивања садржаја елемената, за опажену тенденцију се ипак очекује да буде реална. Предложена класификација звезда из збијених јата може да се прошири у два правца, конкретно на (i) елементе различите од Na и Fe и (ii) друга збијена јата, не само М13.